Perpendicular Emission, Dichroism, and Energy Dependence in Angle-Resolved Photoemission: The Importance of The Final State

M. Dauth,[1] M. Graus,[2] I. Schelter,[1] M. Wießner,[2] A. Schöll,[2] F. Reinert,[2] and S. Kümmel[1]
[1]Theoretical Physics IV, University of Bayreuth, D-95440 Bayreuth, Germany
[2]Experimental Physics VII, University of Würzburg, D-97074 Würzburg, Germany
(Received 24 February 2016; published 24 October 2016)

Angle-resolved photoemission spectroscopy has been developed to a very high accuracy. However, effects that depend sensitively on the state of the emitted photoelectron were so far hard to compute for real molecules. We here show that the real-time propagation approach to time-dependent density functional theory allows us to obtain final-state effects consistently from first principles and with an accuracy that allows for the interpretation of experimental data. In a combined theoretical and experimental study we demonstrate that the approach captures three hallmark effects that are beyond the final-state plane-wave approximation: emission perpendicular to the light polarization, circular dichroism in the photoelectron angular distribution, and a pronounced energy dependence of the photoemission intensity.

DOI: 10.1103/PhysRevLett.117.183001

Photoelectron spectroscopy is one of the most important techniques for characterizing condensed matter systems [1,2]. With rapidly increasing experimental accuracy, increasingly precise insights into the electronic structure have become possible [3,4]. In addition to conventional applications such as the band mapping of solids [5,6], angle-resolved photoemission spectroscopy (ARPES) has become an invaluable tool for studying organic semiconductors and their interfaces [7–9]. It can, e.g., quantify hybridization and band dispersion effects of adsorbed molecular films and can reveal the structure of molecular orbitals [10–19]. Yet, as photoemission is an involved many-body process [2,20–22], the interpretation of experiments relies on theoretical models. Evaluating the commonly assumed one step Fermi's golden rule transition [21,22] requires the initial and the final state. For many prototype organic semiconductors, the initial state has successfully been approximated under the assumption that the photoelectron stems from a single molecular orbital [10,11,13,14,19,22]. Assuming the final state of the emitted electron to be a plane wave (PW) is not only computationally straightforward but under certain conditions [11,23] also leads to a fascinating interpretation of ARPES experiments: The transition matrix element reduces to the Fourier transform $\tilde{\varphi}_i(\mathbf{k})$ of the molecular orbital $\varphi_i(\mathbf{r})$ from which the electron is emitted. Thus, the photoemission intensity,

$$I(k_x, k_y) \propto |\mathbf{A}\cdot\mathbf{k}|^2 |\tilde{\varphi}_i(\mathbf{k})|^2_{k=\text{const}}, \quad (1)$$

finds a powerful interpretation [11]: It reveals the structure of orbital densities on a hemisphere of constant kinetic energy in momentum space [11]. Here, $\mathbf{k}$ denotes the momentum of the photoelectron and $\mathbf{A}$ the vector potential of the ionizing electromagnetic field which also determines the polarization direction of the field. Equation (1) has been used with great success for organic molecular films in the past years [10–19].

Yet, it is well known that important photoemission effects are beyond the PW approximation [18,19,24,25]. A more accurate description of final state effects can be achieved, for instance, with the independent atomic center approximation, (continuum) multiple scattering X_α approaches, frozen-core Hartree-Fock final states, and time reversed low-energy-electron-electron-diffraction (LEED) states [11,20,23,26–33]. Many approaches of this type rely on combining a static single particle concept—often ground-state density functional theory (DFT)—with a model description of the final state.

In this paper we show that simulating the photoemission process in real time within the framework of time-dependent density functional theory (TDDFT) incorporates very important experimentally observed final-state effects. The approach avoids model assumptions about initial and final state and leads to a consistent DFT-based description of photoemission. The emission dynamics emerges naturally including interaction effects between the outgoing electron and the remaining molecule. In this way the need for explicitly evaluating transition matrix elements, which would require a quasiparticle initial state and a fully interacting final state [22,34], is sidestepped.

Specifically, we demonstrate that the real-time description captures three important effects: First, photoemission perpendicular to the light polarization direction, second, circular dichroism in the angular distribution (CDAD) of photoelectrons, and third, the dependence of the emission pattern on the energy of the photoelectron. These effects are missed by the PW approximation: The polarization factor in Eq. (1) strictly forbids intensity in planes perpendicular to the light polarization, a fixed parallel alignment $\mathbf{A}\|\mathbf{k}$ as

preferred by Eq. (1) is not possible for circularly polarized light, and the energy dependence obtained from Eq. (1) is typically much too weak, as it only stems from evaluating the Fourier transform of the orbital on hemispheres of different radii [35].

However, a reliable description of beyond-PW effects is decisive, as exemplified by the following example: In orbital density mapping, one tries to associate the experimentally observed ARPES intensity to one [10,11] or several [13,14] orbitals. As shown in Fig. 1 and discussed in detail below, the PW ansatz can completely miss pronounced spots of intensity. Based on the PW ansatz one would thus associate the wrong orbital with the observed intensity or would wrongly assume contributions from several orbitals in order to explain the intensity pattern. Thus, one would grossly mispredict the studied system's electronic structure. In order to avoid such mistakes, a theoretically consistent approach that allows us to go beyond the PW ansatz, yet is computationally feasible enough to be applicable to true systems, is of great conceptual and practical importance. TDDFT offers the distinct advantage of a favorable ratio of accuracy to computational efficiency.

Different suggestions for simulating photoemission with TDDFT have been made [36–41]. The technique that we rely on here has been pioneered by Pohl *et al.* [38]. Propagating a system's Kohn-Sham (KS) orbitals in real-time on a real-space grid is an established powerful technique [40,42–44]. In our calculations the electronic dynamics is driven by an external electrical dipole field that corresponds to a specific photon energy, polarization, and incidence direction. When the field is large enough it can ionize the system. A fraction of the electron density, represented by the occupied TD KS orbitals, is then traveling away from the molecule. This outgoing density can be understood as originating from a superposition of plane waves. A Fourier transform of the KS orbitals $\varphi_i(\mathbf{R}_D, t)$ recorded at an observation point $\mathbf{R}_D$ far away from the system's center from time t to frequency ω renders a spectral decomposition of the outgoing kinetic energy components. Detecting a photoelectron emitted from a certain state at $\mathbf{R}_D$ is proportional to the probability amplitude [38,45]

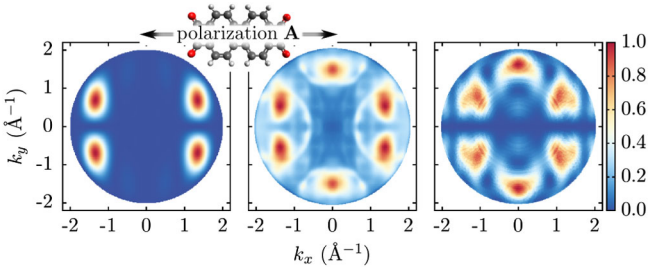

FIG. 1. ARPES maps corresponding to the PTCDA highest occupied molecular orbital (HOMO). Left: plane-wave result; middle: experiment; right: real-time propagation result.

$$I_i \propto |\varphi_i(\mathbf{R}_D, E_{kin} = \hbar\omega)|^2. \quad (2)$$

The total intensity can be calculated by summing up the contributions from all occupied orbitals. By distributing many detection points on a hemisphere, the scheme can record ARPES signals. We recently [45,46] were able to go beyond earlier work on small sodium clusters [38,47,48] and implemented this technique in combination with nonlocal norm-conserving pseudopotentials [49,50], a diligent choice of the required absorbing boundary conditions [51] and an efficient real-space grid parallelization [46]. These aspects are crucial for the present study in order to achieve the very high accuracy that is needed in the computations. They allow us to study the same complex molecules as in recent ARPES experiments and we can capture electron dynamics over extended regions of space. For the perylene-3,4,9,10-tetracarboxylic dianhydride (PTCDA) calculations we in practice used an equally spaced real-space grid with a spacing of $\Delta r = 0.38a_0$ and a radius of $R = 40a_0$. A timestep of $\Delta t = 0.002$ fs was employed with a Crank-Nicholson propagator [52]. The intensity of the incoming light was ramped to a constant intensity of 10^9 W/cm^2 within 0.5 fs and remained constant throughout the total propagation time of $T = 50$ fs. The photoemission signals were evaluated at a detection radius of $R_D = 27a_0$. Further technical details can be found in the Supplemental Material [51], which includes Refs. [53–55], and Ref. [45].

In the following we show that the real-time approach remedies all of the three major restrictions of the PW approximation. In a first step we demonstrate that it can describe electron emission that is not parallel to the field vector. The experimental geometry was in this case chosen such that the light polarization is purely parallel to the long molecular axis, denoted as x axis, of the PTCDA molecules, which are azimuthally aligned in the so-called brick wall monolayer on Ag(110) [56–59]. We refer to the short axis in the molecular plane as the y axis. With this setup, the $\mathbf{A}\|\mathbf{k}$ condition is fulfilled for emission along the x direction and the PW approximation cannot yield any photoemission intensity at $k_x \approx 0$ Å^{-1}. This is reflected in the momentum map on the left of Fig. 1 which we calculated using the PW approximation, the HOMO in the local-density approximation (LDA), and a photoelectron momentum of $|\mathbf{k}| = 2.0$ Å^{-1}. Turning towards our experimentally recorded ARPES spectrum, shown in the middle of Fig. 1, however, reveals that there is significant emission perpendicular to the light polarization: Two bright spots of intensity occur around $k_x \approx 0$ Å^{-1} and $k_y \approx \pm 1.5$ Å^{-1}. The PW approximation completely misses these spots. The ARPES pattern from the real-time approach is displayed on the right of Fig. 1. It was obtained by propagating the KS orbitals of an isolated PTCDA molecule under the influence of an ionizing field with a polarization vector aligned in the x direction and a frequency corresponding to a photon energy of $\hbar\omega = 27$ eV [51], i.e., consistent

with experiment. We again used the LDA and evaluated Eq. (2) for the HOMO. Clearly, the real-time approach captures the emission perpendicular to the light polarization: All six of the experimentally recorded spots of bright intensity are reproduced, and specifically the ones at $k_x \approx 0$ Å^{-1}, $k_y \approx \pm 1.5$ Å^{-1}. The comparison also reveals that there are differences in some of the smaller features: the experimental data include additional arc-shaped features stemming from the sp bands of the silver substrate, and the shape of the spots is not identical. These differences reflect that both experimentally and computationally, obtaining the accuracy for such detailed comparisons is a challenge. For instance, small reflections from the boundary can remain in the calculations and can slightly distort the low intensity regions. However, there is no doubt that in both theory and experiment, pronounced emission perpendicular to the light polarization is observed.

Encouraged by this success we look at a yet more challenging effect, namely differences in the photoemission signal that result from different circular light polarizations. Studies on adsorbed diatomic molecules suggest that here the photoelectron angular distribution is largely governed by interference effects of partial-wave components of the final state [60–62]. Yet, constructing an appropriate final-state approximation for extended molecules is technically and conceptually challenging. Nonetheless there is an urgent need for theoretical access to photon helicity driven ARPES due to the fascinating insights that can be obtained in this way. For instance, dichroism experiments revealed information about the phase symmetry of molecular orbitals [18], and circular dichroism is one of the candidates for explaining the origin of the homochirality of organic molecules which is relevant for the development of life [63].

A necessary criterion for observing CDAD in photoemission is a definite handedness of the entire system. Whereas chiral molecules, with amino acids and further biomolecules as prominent examples, inherently provide a handedness [63–65], the required breaking of inversion symmetry can be implemented by the overall experimental geometry also for nonchiral molecules [60]. Thereby, the ordered monolayer structure of the molecular semiconductors provides a first distinct axis, while the other directions are determined by the photon incidence and the photoemission direction.

In this spirit we probe PTCDA with right circularly polarized (RCP) light and left circularly polarized (LCP) light with an energy of $\hbar\omega = 20$ eV. We set the incidence direction of the photons in the yz plane with an angle of 65° counted from the surface plane normal as displayed in Fig. 2(b). The polarization vector rotates in a plane perpendicular to the incidence direction. Our first observation (both in experiment and calculation) is an increased intensity for photoelectrons emitted in the direction of the polarization plane with $k_y > 0$ Å^{-1} as seen in Figs. 2(a) and 2(c). While this finding is also predicted by the PW approach, the latter results in identical ARPES patterns for LCP and RCP which are symmetrical to $k_x = 0$ Å^{-1} [51]. In contrast, the emission obtained in the real-time propagation has its strongest intensity at about $k_x = 1.4$ Å^{-1} and $k_y = 0.7$ Å^{-1} for LCP, as seen in the upper left part of Fig. 2(a), and when switching the polarization to RCP, as shown in the upper right part of Fig. 2(a), this feature changes sides to $k_x = -1.4$ Å^{-1} and $k_y = 0.7$ Å^{-1}: The whole LCP spectrum equals the RCP one mirrored at the $k_x = 0$ axis. Comparing this to the experimental situation, displayed in the lower row of Fig. 2(a), shows that again the real-time approach captures the relevant experimental features: There are four spots of preferred emission, each one with a different intensity, and upon reversing the helicity, the

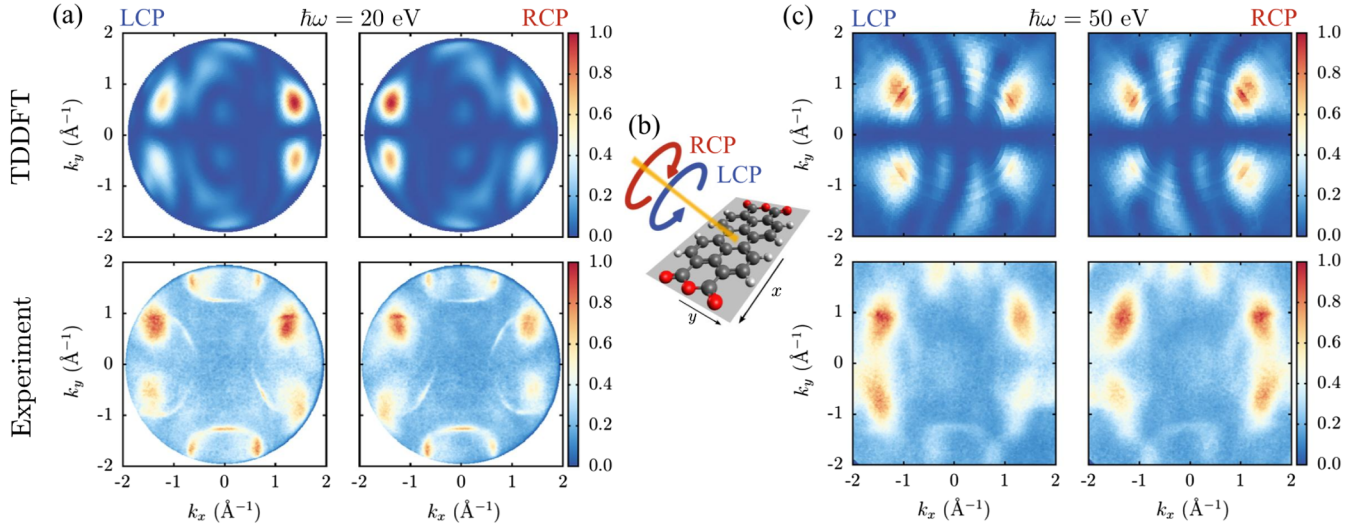

FIG. 2. ARPES maps corresponding to the PTCDA HOMO at $\hbar\omega = 20$ eV (a) and 50 eV (c). Upper row: real-time propagation. Lower row: experiment. Within each panel, LCP spectra are on the left and RCP on the right. Middle panel (b): geometry.

observed pattern is mirrored at the $k_x = 0$ Å^{-1} axis. Note that the LCP and RCP data were obtained in separate, independent calculations and experiments, respectively. That the panels in the upper row in Figs. 2(a) and 2(c) look like pairwise mirror images is a result of the calculations and attests their numerical accuracy. Comparing theory and experiment in detail we note that the intensity difference between the spots at $k_x = 1.4$ Å^{-1}, $k_y = 0.7$ Å^{-1} and $k_x = -1.4$ Å^{-1}, $k_y = 0.7$ Å^{-1} in Fig. 2(a) is more pronounced in the calculations than in the experiment. The influence of the Ag substrate, which is again visible in the experiment, may explain such differences. However, given that recording a subtle observable like dichroism from a monolayer of medium sized molecules is a serious challenge; the qualitative agreement of theory and experiment is noteworthy.

When changing the energy of the incident photons from 20 to 50 eV, we observe a distinct change in the observed ARPES pattern. This pronounced dependence on the kinetic energy of the photoelectron is the third important final-state effect. The lower part of Fig. 2(c) shows the experimental ARPES intensities for a photon energy of $\hbar\omega = 50$ eV, i.e., at considerably higher photoelectron energy than in Fig. 2(a). The upper two panels show the corresponding result from the real-time propagation approach. For computing the latter, the change of the photoelectron energy was easily achieved by simply changing the frequency of the applied external field.

Comparing, e.g., the top left panels of Figs. 2(c) and 2(a) shows that the change of photon energy reverses the observed intensity pattern: The two bright spots that appear on the right side (i.e., $k_x > 0$ Å^{-1}) in the LCP part of Fig. 2(a) appear on the left side (i.e., $k_x < 0$ Å^{-1}) in the LCP part of Fig. 2(c). The same pattern reversal is also seen in the RCP signals. The ability to theoretically predict changes in the intensity patterns—within the accuracy limits of TDLDA—upon varying the photoelectron energy is a consequence of the "automatic" adaption of the photoelectron's state within the real-time approach. As shown in the Supplemental Material [51], this effect is missed completely in the plane-wave approximation. There we also show that the circular dichroism observed experimentally for a different photon incident direction and for the (partially) filled lowest unoccupied molecular orbital of PTCDA is captured by the real-time approach; i.e., the agreement is found not only for the HOMO.

Close inspection of Fig. 2(c) shows that theory and experiment again somewhat differ for some of the less intense features. As mentioned previously, we expect certain differences due to influences of the Ag substrate and finite resolution in the experiment, and remaining quantum mechanical reflections or LDA limitations in the calculations. Therefore, in order to demonstrate the accuracy and generality of the real-time approach beyond the PTCDA molecule, we compare to established reference results for a completely different system: For adsorbed CO molecules, a significant energy dependence of the circular dichroism has been reported [60,61,66,67].

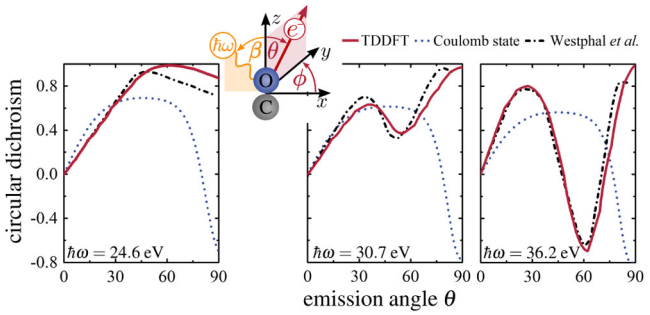

FIG. 3. CDAD intensities for the CO molecule for $\beta = 50°$ and $\phi = 90°$; the black dash-dotted line shows the data [66] from Westphal *et al.*

Figure 3 compares the normalized CDAD intensities, $I_{\mathrm{CDAD}} = (I_{\mathrm{LCP}} - I_{\mathrm{RCP}})/(I_{\mathrm{LCP}} + I_{\mathrm{RCP}})$, of the 4σ orbital of a single CO molecule from the real-time propagation with calculations using frozen-core Hartree-Fock final states [30,61,66], which were calculated by iteratively solving the Lippmann-Schwinger equation. Also shown are results for continuum final states of the bare Coulomb potential corresponding to a single positive charge. The setup is displayed in the inlay of Fig. 3 and has been adopted from Ref. [66]. The real-time approach is close to the reference results for all three photon energies, and we presently cannot tell which approach's limitations are responsible for the small deviations seen for large angles in the left panel. The Coulomb final state results, on the other hand, disagree noticeably, demonstrating that the final state question here is a nontrivial one.

In conclusion, we have demonstrated that the real-time approach to DFT allows us to go beyond the PW final-state approximation in a consistent manner. It opens up theoretical access to important ARPES features. In particular we have shown that three prominent effects are correctly described: emission perpendicular to the light polarization, circular dichroism in the photoelectron angular distribution, and a pronounced energy dependence of the photoemission intensity. Our work indicates that final state properties may also be relevant in several observations in photoemission [33,68] which cannot be described by first principle calculations of the initial state alone.

S. K., I. S., and M. D. acknowledge support by Deutsche Forschungsgemeinschaft (DFG) Graduiertenkolleg 1640 and the Bavarian State Ministry of Science, Research, and the Arts for the Collaborative Research Network "Solar Technologies go Hybrid." A. S. and F. R. thank the DFG (Grants No. GRK1221, No. SCHO-1260/4-1, No. SCHO-1260/5-1, and No. RE1469/9-1) for support. We acknowledge support during the experiments by V. Feyer and P. Nigge.

[1] F. Reinert and S. Hüfner, New J. Phys. **7**, 97 (2005).
[2] L. Kronik and S. Kümmel, in *Topics in Current Chemistry*, edited by C. D. Valentin, S. Botti, and M. Cococcioni (Springer, Berlin-Heidelberg, 2014).
[3] S.-M. Huang, S.-Y. Xu, I. Belopolski, C.-C. Lee, G. Chang, B. Wang, N. Alidoust, G. Bian, M. Neupane, C. Zhang, S. Jia, A. Bansil, H. Lin, and M. Z. Hasan, Nat. Commun. **6**, 7373 (2015).
[4] T. Kondo *et al.*, Nat. Commun. **6**, 10042 (2015).
[5] P. Aebi, R. Fasel, D. Naumovic, J. Hayoz, T. Pillo, M. Bovet, R. Agostino, L. Patthey, L. Schlapbach, F. Gil, H. Berger, T. Kreutz, and J. Osterwalder, Surf. Sci. **402–404**, 614 (1998).
[6] A. Damascelli, H. Zahid, and S. Zhi-Xun, Rev. Mod. Phys. **75**, 473 (2003).
[7] N. Ueno and S. Kera, Prog. Surf. Sci. **83**, 490 (2008).
[8] S. Braun, W. R. Salaneck, and M. Fahlman, Adv. Mater. **21**, 1450 (2009).
[9] A. Kahn, Mater. Horiz. **3**, 7 (2016).
[10] S. Kera, S. Tanaka, H. Yamane, D. Yoshimura, K. K. Okudaira, K. Seki, and N. Ueno, Chem. Phys. **325**, 113 (2006).
[11] P. Puschnig, S. Berkebile, A. J. Fleming, G. Koller, K. Emtsev, T. Seyller, J. D. Riley, C. Ambrosch-Draxl, F. P. Netzer, and M. G. Ramsey, Science **326**, 702 (2009).
[12] J. Ziroff, F. Forster, A. Schöll, P. Puschnig, and F. Reinert, Phys. Rev. Lett. **104**, 233004 (2010).
[13] M. Dauth, T. Körzdörfer, S. Kümmel, J. Ziroff, M. Wiessner, A. Schöll, F. Reinert, M. Arita, and K. Shimada, Phys. Rev. Lett. **107**, 193002 (2011).
[14] P. Puschnig, E.-M. Reinisch, T. Ules, G. Koller, S. Soubatch, M. Ostler, L. Romaner, F. S. Tautz, C. Ambrosch-Draxl, and M. G. Ramsey, Phys. Rev. B **84**, 235427 (2011).
[15] B. Stadtmüller, M. Willenbockel, E. M. Reinisch, T. Ules, F. C. Bocquet, S. Soubatch, P. Puschnig, G. Koller, M. G. Ramsey, F. S. Tautz, and C. Kumpf, Europhys. Lett. **100**, 26008 (2012).
[16] M. Wießner, J. Kübert, V. Feyer, P. Puschnig, A. Schöll, and F. Reinert, Phys. Rev. B **88**, 075437 (2013).
[17] D. Lüftner, T. Ules, E. M. Reinisch, G. Koller, S. Soubatch, F. S. Tautz, M. G. Ramsey, and P. Puschnig, Proc. Natl. Acad. Sci. U.S.A. **111**, 605 (2014).
[18] M. Wießner, D. Hauschild, C. Sauer, V. Feyer, A. Schöll, and F. Reinert, Nat. Commun. **5**, 4156 (2014).
[19] S. Weiß, D. Lüftner, T. Ules, E. M. Reinisch, H. Kaser, A. Gottwald, M. Richter, S. Soubatch, G. Koller, M. G. Ramsey, F. S. Tautz, and P. Puschnig, Nat. Commun. **6**, 8287 (2015).
[20] P. J. Feibelman and D. E. Eastman, Phys. Rev. B **10**, 4932 (1974).
[21] J. B. Pendry, Surf. Sci. **57**, 679 (1976).
[22] M. Dauth, M. Wießner, V. Feyer, A. Schöll, P. Puschnig, F. Reinert, and S. Kümmel, New J. Phys. **16**, 103005 (2014).
[23] W. D. Grobman, Phys. Rev. B **17**, 4573 (1978).
[24] N. Richardson, Chem. Phys. Lett. **102**, 390 (1983).
[25] A. M. Bradshaw and D. P. Woodruff, New J. Phys. **17**, 013033 (2015).
[26] J. W. Gadzuk, Phys. Rev. B **10**, 5030 (1974).
[27] D. Dill and J. L. Dehmer, J. Chem. Phys. **61**, 692 (1974).
[28] A. Liebsch, Phys. Rev. Lett. **32**, 1203 (1974).
[29] Y.-i. Suzuki and T. Suzuki, J. Phys. Chem. A **112**, 402 (2008).
[30] R. R. Lucchese, G. Raseev, and V. McKoy, Phys. Rev. A **25**, 2572 (1982).
[31] P. Krüger, F. DaPieve, and J. Osterwalder, Phys. Rev. B **83**, 115437 (2011).
[32] A. X. Gray, C. Papp, S. Ueda, B. Balke, Y. Yamashita, L. Plucinski, J. Minár, J. Braun, E. R. Ylvisaker, C. M. Schneider, W. E. Pickett, H. Ebert, K. Kobayashi, and C. S. Fadley, Nat. Mater. **10**, 759 (2011).
[33] M. R. Scholz, J. Sanchez-Barriga, J. Braun, D. Marchenko, A. Varykhalov, M. Lindroos, Y. J. Wang, H. Lin, A. Bansil, J. Minár, H. Ebert, A. Volykhov, L. V. Yashina, and O. Rader, Phys. Rev. Lett. **110**, 216801 (2013).
[34] M. Walter and H. Häkkinen, New J. Phys. **10**, 043018 (2008).
[35] Many valence orbitals are rather smooth in the relevant parts of $\mathbf{k}$ space.
[36] C. A. Ullrich, P.-G. Reinhard, and E. Suraud, J. Phys. B **30**, 5043 (1997).
[37] U. De Giovannini, D. Varsano, M. A. L. Marques, H. Appel, E. K. U. Gross, and A. Rubio, Phys. Rev. A **85**, 062515 (2012).
[38] A. Pohl, P.-G. Reinhard, and E. Suraud, Phys. Rev. Lett. **84**, 5090 (2000).
[39] P. M. Dinh, P. Romaniello, P.-G. Reinhard, and E. Suraud, Phys. Rev. A **87**, 032514 (2013).
[40] M. Mundt and S. Kümmel, Phys. Rev. B **76**, 035413 (2007).
[41] V. Véniard, R. Taïeb, and A. Maquet, Laser Phys. **13**, 465 (2003).
[42] K. Yabana and G. F. Bertsch, Phys. Rev. B **54**, 4484 (1996).
[43] F. Calvayrac, P.-G. Reinhard, and E. Suraud, Ann. Phys. (N.Y.) **255**, 125 (1997).
[44] A. Castro, H. Appel, M. Oliveira, C. Rozzi, X. Andrade, F. Lorenzen, M. A. L. Marques, E. K. U. Gross, and A. Rubio, Phys. Status Solidi B **243**, 2465 (2006).
[45] M. Dauth and S. Kümmel, Phys. Rev. A **93**, 022502 (2016).
[46] I. Schelter and S. Kümmel (unpublished).
[47] P. Wopperer, B. Faber, P. M. Dinh, P.-G. Reinhard, and E. Suraud, Phys. Rev. A **82**, 063416 (2010).
[48] P. Wopperer, P. M. Dinh, E. Suraud, and P.-G. Reinhard, Phys. Rev. A **85**, 015402 (2012).
[49] N. Troullier and J. L. Martins, Phys. Rev. B **43**, 1993 (1991).
[50] The cutoff radii of our LDA-consistent pseudopotentials were $r_c = 1.39a_0$ for H, $1.09a_0$ for C, and $1.10a_0$ for O.
[51] See Supplemental Material at http://link.aps.org/supplemental/10.1103/PhysRevLett.117.183001 for details.
[52] A. Castro, M. A. L. Marques, and A. Rubio, J. Chem. Phys. **121**, 3425 (2004).
[53] D. E. Manolopoulos, J. Chem. Phys. **117**, 9552 (2002).
[54] T. Gonzalez-Lezana, E. J. Rackham, and D. E. Manolopoulos, J. Chem. Phys. **120**, 2247 (2004).
[55] P. Schaffhauser and S. Kümmel, Phys. Rev. B **93**, 035115 (2016).
[56] C. Seidel, C. Awater, X. Liu, R. Ellerbrake, and H. Fuchs, Surf. Sci. **371**, 123 (1997).
[57] K. Glöckler, C. Seidel, A. Soukopp, M. Sokolowski, E. Umbach, M. Bohringer, R. Berndt, and W. Schneider, Surf. Sci. **405**, 1 (1998).

[58] Y. Zou, L. Kilian, A. Schöll, T. Schmidt, R. Fink, and E. Umbach, Surf. Sci. **600**, 1240 (2006).
[59] M. Wießner, D. Hauschild, A. Schöll, F. Reinert, V. Feyer, K. Winkler, and B. Krömker, Phys. Rev. B **86**, 045417 (2012).
[60] G. Schönhense, Phys. Scr. **T31**, 255 (1990).
[61] R. L. Dubs, S. N. Dixit, and V. McKoy, Phys. Rev. Lett. **54**, 1249 (1985).
[62] I. Dreissigacker and M. Lein, Phys. Rev. A **89**, 053406 (2014).
[63] N. Böwering, T. Lischke, B. Schmidtke, N. Müller, T. Khalil, and U. Heinzmann, Phys. Rev. Lett. **86**, 1187 (2001).
[64] B. Ritchie, Phys. Rev. A **13**, 1411 (1976).
[65] I. Powis, J. Chem. Phys. **112**, 301 (2000).
[66] C. Westphal, J. Bansmann, M. Getzlaff, G. Schönhense, N. A. Cherepkov, M. Braunstein, V. McKoy, and R. L. Dubs, Surf. Sci. **253**, 205 (1991).
[67] C. Westphal, J. Bansmann, M. Getzlaff, and G. Schönhense, Phys. Rev. Lett. **63**, 151 (1989).
[68] H. Maaß, H. Bentmann, C. Seibel, C. Tusche, S. V. Eremeev, T. R. Peixoto, O. E. Tereshchenko, K. A. Kokh, E. V. Chulkov, J. Kirschner, and F. Reinert, Nat. Commun. **7**, 11621 (2016).